J Mater Sci (2015) 50:6498–6509
DOI 10.1007/s10853-015-9209-4

Structural evolution, mechanical properties, and electronic structure of Al–Mg–Si compounds from first principles

Bo Zhang[1] · Lailei Wu[2] · Biao Wan[2] · Jingwu Zhang[2] · Zhihong Li[1] · Huiyang Gou[2]

Received: 10 June 2015 / Accepted: 24 June 2015 / Published online: 3 July 2015

Abstract Nano-sized precipitates in Al–Mg–Si alloys can effectively increase the mechanical property of these alloys. However, nanoscale dimensions and orientation variations greatly impede the understanding of crystal structures and phase relations of precipitates. In this paper, the structural stability, mechanical, and electronic properties of twelve Al–Mg–Si compounds in Al–Mg–Si alloys are examined systematically using first-principles calculations. The calculated results of Mg_2Si and MgAlSi agree well with the previous experimental and theoretical results. The Mg_4Si_7 with $P\bar{1}$ symmetry, $MgAl_2Si_2$ with $C2/m$ symmetry, and Mg_4AlSi_3 with $Pccn$ symmetry are identified as the more energetically and mechanically favorable phases suggested by our calculations. According to the predictions, $MgSi_2$ and MgAlSi exhibit higher bulk moduli, 73.1 and 67.7 GPa, due to the tightly bounding Si–Si/Si–Al covalent networks.

Bo Zhang, and Lailei Wu have contributed equally to this work.

Electronic supplementary material The online version of this article (doi:10.1007/s10853-015-9209-4) contains supplementary material, which is available to authorized users.

✉ Zhihong Li
lizhihong@tju.edu.cn

✉ Huiyang Gou
huiyang.gou@gmail.com

Bo Zhang
zhangbo812@tju.edu.cn

[1] Key Laboratory of Advanced Ceramics and Machining Technology of Ministry of Education, School of Materials Science and Engineering, Tianjin University, Tianjin 300072, China

[2] Key Laboratory of Metastable Materials Science and Technology, College of Material Science and Engineering, Yanshan University, Qinhuangdao 066004, China

Introduction

Al–Mg–Si alloys are extensively used in many industrial applications, such as lightweight construction, automotive, aircraft, and architecture, because of the excellent formability, mechanical strength, corrosion resistance, and weldability [1–3]. During a specific heating treatment process (known as aging hardening), the presence of diverse nano-sized needle- or plate-like metastable precipitates from the aluminum matrix greatly hinders the movement of dislocations and thus enhances the mechanical property of alloys [4]. Generally, the generic precipitation follows the sequence of SSSS → Mg/Si clusters → GP-zones → pre-β″ → β″ (Mg_5Si_6) → {U1, U2, B′, β′} → β (Mg_2Si, stable), where SSSS refers to a supersaturated solid solution and GP-zones are aggregates of solute atoms in the aluminum matrix. Among the precipitations, β″ phase, generally present in alloys aged to peak hardness, has been determined to be a monoclinic structure with an ideal composition, Mg_5Si_6 [4]. However, in specific age-hardening process, low annealing temperatures and short annealing time limit the appearance of β″ phase, and thus the pre-β″ phase is formed with varied composition other than Mg_5Si_6, e.g., Mg_4Si_7, $Mg_2Al_3Si_6$, and Mg_4AlSi_6 [5, 6]. The phases U1, U2, and B′ refer to "type A", "type B", and ''type C'' precipitates, respectively [7]. Furthermore, rod-like β′ is reported to appear in over-aged specimens and is determined to be hexagonal phase with a composition of Mg_9Si_5 [2]. The equilibrium phase in this system, the β phase, Mg_2Si, has a cubic anti-fluorite (CaF_2) structure (space group $Fm3m$). Very recently, two new compounds, $(Mg_9Si_5)_{HP}$ and $(Mg_4AlSi_3)_{HP}$ are reported by Ji

et al. [8] under high pressure (5 GPa) and high temperature (900–1100 °C) conditions. In general, the microstructures of clusters and precipitates are often investigated by atom probe tomography [1, 9, 10] and high-resolution transmission electron microscopy [11, 12]. Nevertheless, small grain-size and many possible orientations of precipitates may limit the determinations of structure and physical properties.

First-principles calculation is a valuable prediction approach to understand precipitate energetics and studying their structural transformations [13, 14]. The bonding characteristics of the key precipitates in Al–Mg–Si alloys were investigated by Frøseth et al. [15] using augmented plane-wave under the framework of density functional theory calculations about one decade ago. The energetics of most of the precipitates in Al–Mg–Si system was studied by Ravi and Wolverton [6] using density functional-based calculations in both the local density approximations (LDA) and generalized gradient approximations (GGA). van Huis et al. [5, 16] systematically investigated stability and structural relations of the matrix-embedded precipitate phases in the Al–Mg–Si alloys during the evolution process by means of first-principles calculations. Zhao et al. [17] calculated the structure, stability, and finite-temperature thermodynamic properties of the key precipitates in the Al–Mg–Si alloy. Ehlers examined interface configuration stabilities and determined the interfacial energies over the full precipitate cross-section for the phase β″ in the Al–Mg–Si alloy system [14]. Most of the efforts were focused on the thermodynamic stability and structural relationship between the precipitates and the Al matrix. However, to our knowledge, there are no comparative investigations on the mechanical properties and underlying relations between these phases of Al–Mg–Si compounds. Therefore, by means of first-principles calculations based on density functional theory, in this paper, we report the enthalpies of formation, elastic constants, and electron structures of the whole precipitate phases, i.e., pre-β″/(Mg_4AlSi_6, $Mg_2Al_3Si_6$, Mg_4Si_7), β″/Mg_5Si_6, β′/Mg_9Si_5, U1/$MgAl_2Si_2$, U2/MgAlSi, U3/$MgSi_2$ [2], B′/$Mg_9Al_3Si_7$, β/Mg_2Si, and two high pressure phases—$(Mg_9Si_5)_{HP}$ and $(Mg_4AlSi_3)_{HP}$. The systematic studies on the Al–Mg–Si compounds here would help the further understanding of the structural behaviors and mechanical properties of the metastable precipitate phases.

Computational details

First-principles calculations were performed using CASTEP code based on density functional theory (DFT) [18]. The exchange and correlation functions were treated by generalized gradient approximation with the parameterization by Perdew–Burke–Ernzerhof (GGA-PBE) [19, 20]. The electronic configurations of each element were $3s^23p^1$ for Al, $2p^63s^2$ for Mg, and $3s^23p^2$ for Si, respectively. The convergence of calculations is initially checked by a 10 × 10 × 10 *k*-point and cutoff energy of 350 eV. The ground state and elastic constants (C_{ij}) of all considered Al–Mg–Si compounds are then calculated for each fully relaxed structure. Bulk and shear moduli were estimated based on Voight–Reuss–Hill (VRH) approximation [21]. Elastic moduli and Poisson's ratio were obtained based on the relationship: $E = 9BG/(3B + G)$, $\nu = (3B - 2G)/(6B + 2G)$. The universal elastic anisotropy index (A^U) [22] is obtained from the B and G of Voigt and Reuss with the equation: $A^U = 5G_V/G_R + B_V/B_R - 6$.

Structural stability

Mechanical stability, a necessary condition for a stable crystal to exist in experiments, was firstly checked for all of the precipitates according to the Born–Huang criterion [23, 24]. The mechanical stability criteria are given as follows:

For cubic phase,

$$C_{11} > 0,\ C_{44} > 0,\ C_{11} > |C_{12}|,\ (C_{11} + 2C_{12}) > 0;$$

For hexagonal phase,

$$C_{44} > 0,\ C_{11} > |C_{12}|,\ (C_{11} + 2C_2)C_{33} > 2C_{13}C_{13};$$

For tetragonal phase,

$$C_{11} > 0, C_{33} > 0, C_{44} > 0, C_{66} > 0, (C_{11} - C_{12}) > 0,$$
$$(C_{11} + C_{33} - 2C_{13}) > 0, [2(C_{11} + C_{12}) + C_{33} + 4C_{13}] > 0;$$

For trigonal phase,

$$C_{11} > 0,\ C_{33} > 0,\ C_{44} > 0,\ (C_{11} + C_{12})C_{33} > 2C_{13}C_{13},$$
$$(C_{11} - C_{12})C_{44} > 2C_{14}C_{14}$$

For orthorhombic phase,

$$C_{11} > 0,\ C_{22} > 0,\ C_{33} > 0,\ C_{44} > 0,\ C_{55} > 0,\ C_{66} > 0,$$
$$[C_{11} + C_{22} + C_{33} + 2(C_{12} + C_{13} + C_{23})] > 0,$$
$$(C_{11} + C_{22} - 2C_{12}) > 0,$$

$$(C_{11} + C_{33} - 2C_{13}) > 0,\ (C_{22} + C_{33} - 2C_{23}) > 0;$$

For monoclinic phase,

$$C_{11} > 0,\ C_{22} > 0,\ C_{33} > 0,\ C_{44} > 0,\ C_{55} > 0,\ C_{66} > 0,$$
$$[C_{11} + C_{22} + C_{33} + 2(C_{12} + C_{13} + C_{23})] > 0,$$
$$(C_{33}C_{55} - C_{35}C_{35}) > 0,$$

$$(C_{44}C_{66} - C_{46}C_{46}) > 0,\ (C_{22} + C_{33} - 2C_{23}) > 0,$$
$$[C_{22}(C_{33}C_{55} - C_{35}C_{35}) + 2C_{23}C_{25}C_{35} - C_{23}C_{23}C_{55}$$
$$- C_{25}C_{25}C_{33}] > 0,$$

Table 1 Calculated elastic constants C_{ij} (in GPa) of considered Al–Mg–Si compounds

Phase	S.G.	C_{11}	C_{22}	C_{33}	C_{44}	C_{55}	C_{66}	C_{12}	C_{13}	C_{23}
pre-β″/Mg_4AlSi_6	*C*2/*m*	105.8	128.0	105.1	5.0	33.4	29.2	23.1	56.0	22.8
pre-β″/$Mg_2Al_3Si_6$	*C*2/*m*	163.2	163.6	137.1	23.6	37.5	68.9	38.8	18.2	−1.8
pre-β″/Mg_4Si_7	$P\bar{1}$	145.7	111.0	116.4	17.7	23.8	30.3	22.1	34.7	28.5
	*C*2/*m*	139.0	128.1	89.2	−127.7	40.3	32.5	30.6	49.4	32.8
β″/Mg_5Si_6	*C*2/*m*	132.1	157.6	105.1	13.1	43.4	40.1	32.4	43.2	11.2
U1/$MgAl_2Si_2$	*C*2/*m*	75.7	143.2	99.0	14.3	41.0	14.4	49.1	51.4	30.5
	$P\bar{3}m1$	62.0	64.5	59.6	10.1	−26.5	46.7			
U2/MgAlSi	*Pnma*	120.5	146.0	110.8	50.3	60.3	52.4	34.7	51.3	30.3
U3/$MgSi_2$	*Imma*	126.9	137.1	125.9	26.2	48.8	42.0	31.8	47.6	55.6
B′/$Mg_9Al_3Si_7$	$P\bar{6}$	98.0		104.9	14.2			26.6	44.6	
β′/Mg_9Si_5	$P6_3/m$	126.8		121.8	23.9			28.2	20.2	
β/Mg_2Si	$Fm\bar{3}m$	113.2			42.4			22.8		
$(Mg_9Si_5)_{HP}$	$P6_3$	100.1		124.5	18.7			46.0	16.0	
$(Mg_4AlSi_3)_{HP}$	*Pccn*	138.2	103.7	129.8	24.6	17.7	18.5	54.3	27.7	13.6
	*P*4/*ncc*	48.03		127.8	20.0		-8.4	123.6	24.0	

$$\{2[C_{15}C_{25}(C_{33}C_{12}-C_{13}C_{23})+C_{15}C_{35}(C_{22}C_{13}-C_{12}C_{23})+C_{25}C_{35}(C_{11}C_{23}-C_{12}C_{13})]-[C_{15}C_{15}(C_{22}C_{33}-C_{23}C_{23})+C_{25}C_{25}(C_{11}C_{33}-C_{13}C_{13})+C_{35}C_{35}(C_{11}C_{22}-C_{12}C_{12})]+C_{55}(C_{11}C_{22}C_{33}-C_{11}C_{23}C_{23}-C_{22}C_{13}C_{13}-C_{12}C_{12}C_{33}+2C_{12}C_{13}C_{23})\}$$

If all the individual elastic moduli of a specific phase are satisfied, the above criteria indicate its stability. The calculated elastic constants of the Al–Mg–Si compounds are given in Table 1. It can be found that pre-β″/$Mg_2Al_3Si_6$, pre-β″/Mg_4AlSi_6, β″/Mg_5Si_6, U2/MgAlSi, U3/$MgSi_2$, B′/$Mg_9Al_3Si_7$, β′/Mg_9Si_5, β/Mg_2Si, and $(Mg_9Si_5)_{HP}$ satisfy the Born–Huang criterion, indicating their mechanical stability. However, pre-β″/Mg_4Si_7 ($C_{44} = -127.7$ GPa), U1/$MgAl_2Si_2$ ($C_{55} = -26.5$ GPa), and $(Mg_4AlSi_3)_{HP}$ ($C_{66} = -8.4$ GPa) are mechanically unstable, which are surprising to appear in the experimental observations [5–8]. To get a further understanding of the structural configurations of pre-β″/Mg_4Si_7, U1/$MgAl_2Si_2$, and $(Mg_4AlSi_3)_{HP}$, 2 × 2 × 2 supercells were conducted to produce mechanically stable phases: $P\bar{1}$-type (Space group number: 2) Mg_4Si_7, *C*2/*m*-type (Space group number: 12) $MgAl_2Si_2$ and *Pccn*-type (Space group number: 56) Mg_4AlSi_3, which are found to be energetically more favorable than the previously identified structures with about 29, 32, and 10 meV/atom, respectively (as shown in Fig. 1a). Further dynamical stability for these structures was also validated, because no soft mode was observed in their phonon curves (as shown in Fig. 1b–d). Considering the small size of precipitates and possible orientations in experiment, $P\bar{1}$-Mg_4Si_7, *C*2/*m*-$MgAl_2Si_2$, and *Pccn*-Mg_4AlSi_3 should be more likely to precipitate and will be discussed in the following sections.

To verify the thermodynamic stability of the considered precipitated phases in the alloys, the formation enthalpies (ΔH_f) are calculated as listed in Table 2 and compared with available experimental and literature first-principles calculation results [5, 6, 17, 25–33]. The formation enthalpy of $Mg_xAl_ySi_z$ phase is defined as

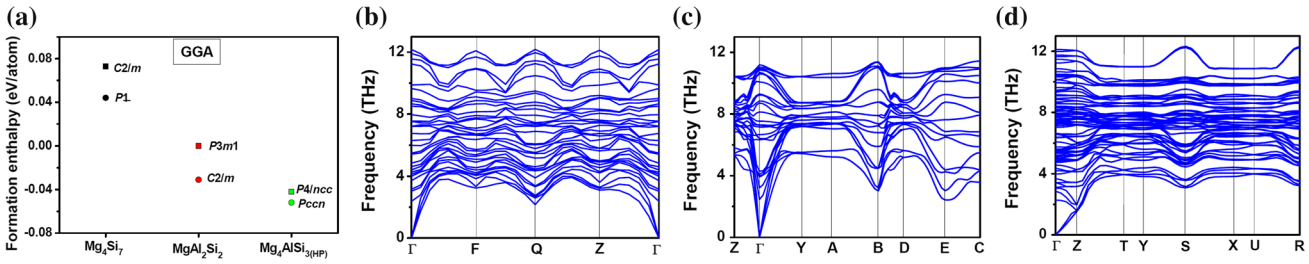

Fig. 1 (color online) Formation enthalpies of our proposed structures of Mg_4Si_7, $MgAl_2Si_2$, and $(Mg_4AlSi_3)_{HP}$ compared with previously identified structures (**a**), and Phonon dispersion curves of $P\bar{1}$-Mg_4Si_7 (**b**), *C*2/*m*-$MgAl_2Si_2$ (**c**), and *Pccn*-$(Mg_4AlSi_3)_{HP}$ (**d**)

Table 2 Calculated enthalpies of A–Mg–Si alloys compared with available theoretical and experimental results

Phase	S.G.	ΔH_f		Method	Reference
		eV/atom	kJ/mol-atom		
pre-β″/Mg_4AlSi_6	Mon.(*C*2/*m*)	0.067	6.46	This work	
			10.8	VASP-GGA	van Huis et al. [5]
			10.0	VASP-GGA	Ravi and Wolverton [6]
pre-β″/$Mg_2Al_3Si_6$	Mon.(*C*2/*m*)	0.102	9.84	This work	
			17.9	VASP-GGA	van Huis et al. [5]
pre-β″/Mg_4Si_7	Tric. ($P\bar{1}$)	0.044	4.25	This work	
	Mon.(*C*2/*m*)	0.073	7.04	This work	
			11.1	VASP-GGA	van Huis et al. [5]
β″/Mg_5Si_6	Mon.(*C*2/*m*)	−0.020	−1.93	This work	
			4.0	VASP-GGA	van Huis et al. [5]
			3.312	GGA	Zhao et al. [17]
			3.5	GGA	Zhang et al. [32]
			3.3	GGA	Ravi and Wolverton [6]
U1/$MgAl_2Si_2$	Mon.(*C*2/*m*)	−0.031	−2.99	This work	van Huis et al. [5]
	$P\bar{3}m1$	0.0001	0.0096		This work
	$P\bar{3}m1$		−2.9	VASP-GGA	van Huis et al. [5]
			−3.1	VASP-GGA	Ravi and Wolverton [6]
			−0.7530	VASP-GGA	Zhao et al. [17]
U2/MgAlSi	Ort.(*Pnma*)	−0.106	−10.23	This work	
			−5.2	VASP-GGA	van Huis et al. [5]
			−5.8	VASP-GGA	Ravi and Wolverton [6]
			−4.506	VASP-GGA	Zhao et al. [17]
U3/$MgSi_2$	Ort.(*Imma*)	0.034	3.28	This work	
			12.7	VASP-GGA	van Huis et al. [5]
B′/$Mg_9Al_3Si_7$	Hex.($P\bar{6}$)	−0.067	−6.46	This work	
			−6.7	VASP-GGA	van Huis et al. [5]
			−6.9		Ravi and Wolverton [6]
β′/Mg_9Si_5	Hex.($P6_3/m$)	−0.127	−12.25	This work	
			−12.7	VASP-GGA	van Huis et al. [5]
			−12.6	VASP-GGA	Zhang et al. [25]
			−11.7	VASP-GGA	Ravi and Wolverton [6]
			−11.552	VASP-GGA	Zhao et al. [17]
β/Mg_2Si	Cub.($Fm\bar{3}m$)	−0.163	−15.73	This work	
			−17.8	VASP-GGA	van Huis et al. [5]
			−18.0	VASP-GGA	Ravi and Wolverton [6]
			−15.667	VASP-GGA	Zhao et al. [17]
			−25.9	Calorimetry	Kubaschewski and Villa [26]
			−27.1	Calorimetry	Gerstein et al. [27]
			−29.7	Calorimetry	Blachnik et al. [28]
			−61.9	Knudsen cell	Caulfield and Hudson [29]
			−27.9	Knudsen cell	Ryabchikov and Mikulinski [30]
			−26.4	EMF	Lukashenko and Eremenko [31]
			−22.2	EMF	Rao et al. [32]
			−21.1	Calorimetry	Feufel et al. [33]
$(Mg_9Si_5)_{HP}$	Hex.($P6_3$)	−0.084	−8.10	This work	

Table 2 continued

Phase	S.G.	ΔH_f		Method	Reference
		eV/atom	kJ/mol-atom		
$(Mg_4AlSi_3)_{HP}$	Ort. (*Pccn*)	−0.052	−5.02	This work	
	Tet.(*P4/ncc*)	−0.042	−4.05	This work	
	Tet.(*P4/ncc*)				

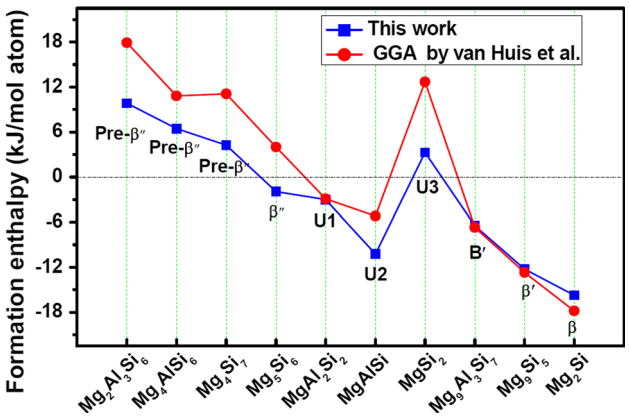

Fig. 2 (color online) Calculated formation enthalpies of the precipitates in Al–Mg–Si alloys comparing with theoretical results in Ref. [5] by GGA

$$\Delta H_{\mathrm{f}} = E_{\mathrm{total}}\left(\mathrm{Mg}_x\mathrm{Al}_y\mathrm{Si}_z\right) - \left(xE_{\mathrm{total}}(\mathrm{Mg}) + yE_{\mathrm{total}}(\mathrm{Al}) + zE_{\mathrm{total}}(\mathrm{Si})\right) \quad (1)$$

where $E_{\mathrm{total}}(\mathrm{Mg}_x\mathrm{Al}_y\mathrm{Si}_z)$ is the total energy of $\mathrm{Mg}_x\mathrm{Al}_y\mathrm{Si}_z$ at equilibrium lattice constants; $E_{\mathrm{total}}(\mathrm{Mg})$, $E_{\mathrm{total}}(\mathrm{Al})$, and $E_{\mathrm{total}}(\mathrm{Si})$ are the calculated total energies of *hcp*-Mg (S.G. $P6_3/mmc$), *fcc*-Al (S.G. *Fm*-3*m*), and *diamond*-Si (S.G. *Fd*-3*m*); and *x*, *y*, and *z* ($x + y + z = 1$) are the atomic fractions of Mg, Si, Al, respectively. Generally, our obtained results agree well with previous ones. Figure 2 shows the formation enthalpies of the precipitated phases in comparison with GGA (VASP) results by van Huis et al. [5]. It can be seen that all three pre-β″ phases (Mg_4Si_7, Mg_4AlSi_6, and $Mg_2Al_3Si_6$) show positive formation enthalpy, which were identified in the early stage during age- hardening process based on both experimental and theoretical results [3, 16, 34, 35]. Following the precipitation sequence, except for $MgSi_2$ (an only theoretically predictive phase and has not been observed experimentally), the formation enthalpy of the metastable precipitates becomes negative, suggesting the stable behaviors against the decomposition into their elemental compositions under ambient conditions. The formation enthalpy of the precipitates follows the sequence of pre-β″ ($Mg_2Al_3Si_6$ > Mg_4AlSi_6 > Mg_4Si_7) > β″/Mg_5Si_6 > {U1/$MgAl_2Si_2$ > B′/$Mg_9Al_3Si_7$ > U2/MgAlSi > β′/Mg_9Si_5} > β/Mg_2Si. Our calculated results also confirmed that Mg_2Si phase has the most negative ΔH (−0.163 eV/atom; −15.73 kJ/mol-atom), verified by experiment as the equilibrium phase. The sequence of the calculated formation enthalpy is quite consistent with the experimental observations [1, 15, 36] and results by van Huis et al. [5]. It is also interesting to know that the structural symmetry of the key precipitates in Al–Mg–Si alloys changes following the precipitation sequence, i.e., from triclinic ($P\bar{1}$-Mg_4Si_7) and monoclinic (*C*2/*m*-$Mg_2Al_3Si_6$; *C*2/*m*-Mg_4AlSi_6, *C*2/*m*-Mg_5Si_6 and *C*2/*m*-$MgAl_2Si_2$) to orthorhombic (*Pnma*-MgAlSi and *Imma*-$MgSi_2$), then hexagonal ($P\bar{6}$-$Mg_9Al_3Si_7$ and $P6_3/m$-Mg_9Si_5), and finally cubic ($Fm\bar{3}m$-Mg_2Si), which may result from the structural stabilization of the temperature-dependent entropic contributions to the free energy.

The calculated structural parameters and Wyckoff positions of different precipitates, after full stress and position relaxation, are shown in Table 3 and Supporting Information. In general, our results are in good accordance with the previous theoretical results [2, 4–6, 8, 14, 37–40]. The lattice constant of *a* of monoclinic Mg_4AlSi_6 deviates by ~12 % comparing with the experimental values, as suggested by Ref. [4], which may result from the interfacial and strain energies generated during precipitate process, influencing the crystal structure of the precipitate phases, the matrix phase, and the interface between them. As shown in Fig. 3, the crystal structures of the pre-β″ phases ($P\bar{1}$-type Mg_4Si_7 in Fig. 3a, Mg_4AlSi_6 in Fig. 3b, and $Mg_2Al_3Si_6$ in Fig. 3c) are composed of corrugated Si layers, and the Si layers are alternately stacked with Mg atoms paralleling to *c* axis. The Si layers can be also viewed as parallelogram-Si_4 (denoted as P-Si_4 later) zigzag chains connected by rhombus-Si_4 (denoted as R-Si_4 later) planar chains. The structures of Mg_4AlSi_6 and $Mg_2Al_3Si_6$ are reasonably built from $P\bar{1}$-type Mg_4Si_7 with Si1, Mg2, and Mg3 atom substituted by Al atoms, respectively. Experimentally, in the precipitation process, Si and Mg tend to form clusters at the beginning. Initially, the clusters will be Si-rich due to its poorer solubility in Al and have higher diffusion speed. Subsequently, Mg will diffuse into the Si-rich clusters to form Mg/Si clusters [41]. Then Al atoms diffusing from the matrix replaced Mg or Si atoms in Mg/Si clusters. The bond lengths of Si–Si in P-Si_4 unit are 2.37

Table 3 Calculated and experimental lattice parameters of considered Al–Mg–Si compounds

Phase	S.G.	Z	Lattice parameter			Ref.	Phase	S.G.	Z	Lattice parameter			Ref.
			a (Å) α	*b* (Å) *β*	*c* (Å) *γ*					*a* (Å) α	*b* (Å) *β*	*c* (Å) *γ*	
pre-β″/Mg_4AlSi_6	Mon.(*C*2/*m*)	2	16.455	3.535 91.5°	7.053	This work	U3/$MgSi_2$	Ort.(*Imma*)	2	6.134	4.134	7.993	This work
			16.53	3.64 91°	6.72	[6]$^{Theo.}$				6.48	4.03	7.84	[14]$^{Theo.}$
			14.60	4.05 105°	6.40	[4]$^{Exp.}$							
pre-β″/ $Mg_2Al_3Si_6$	Mon.(*C*2/*m*)	2	15.039	3.519 107.4°	7.399	This work	B′/$Mg_9Al_3Si_7$	Hex.($P\bar{6}$)	1	10.312	10.312	3.961	This work
			14.60	4.05 105°	6.40	[5]$^{Theo.}$				10.49	10.49	3.79	[6]$^{Theo.}$
			14.78	4.05 107°	6.74	[34]$^{Exp.}$				10.40	10.40	4.01	[39]$^{Exp.}$
pre-β″/Mg_4Si_7	Tric. ($P\bar{1}$)	1	3.640 94.0°	7.298 102.3°	8.025 80.3°	This work	β′/Mg_9Si_5	Hex.($P6_3/m$)	2	7.203	7.203	12.349	This work
	Mon.(*C*2/*m*)	2	15.685	3.603 89.3°	7.155	This work				7.15	7.15	12.15	[2]$^{Theo.}$
	Mon.(*C*2/*m*)		14.60	4.05 105°	6.40	[5]$^{Theo.}$				7.15	7.15	12.15	[2]$^{Exp.}$
β″/Mg_5Si_6	Mon.(*C*2/*m*)	2	15.114	3.995 113.9°	7.391	This work	β/Mg_2Si	Cub.($Fm\bar{3}m$)	4	6.386	6.386	6.386	This work
			15.83	3.98 102°	6.52	[6]$^{Theo.}$				6.35	6.35	6.35	[6]$^{Theo.}$
			15.16	4.05 105°	6.74	[4]$^{Exp.}$				6.34	6.34	6.34	[40]$^{Exp.}$
U1/$MgAl_2Si_2$	Mon.(*C*2/*m*)	2	6.924	4.197 136.5	9.721	This work	$(Mg_9Si_5)_{HP}$	Hex.($P6_3$)	2	12.35	12.35	13.20	This work
	$P\bar{3}m1$	1	4.110	4.110	6.593	This work				12.41	12.41	12.35	[8]$^{Exp.}$
	$P\bar{3}m1$		4.07	4.07	6.68	[6]$^{Theo.}$							
			4.05	4.05	6.74	[37]$^{Exp.}$							
U2/MgAlSi	Ort.(*Pnma*)	4	6.428	3.977	8.453	This work	$(Mg_4AlSi_3)_{HP}$	Ort. (*Pccn*)	4	6.275	6.966	13.679	This work
		4	6.60	4.04	8.04	[6]$^{Theo.}$		Tet.(*P*4/*ncc*)	4	6.598	6.598	13.637	This work
			6.75	4.05	7.94	[38]$^{Exp.}$		Tet.(*P*4/*ncc*)		6.72	6.72	13.52	[8]$^{Exp.}$

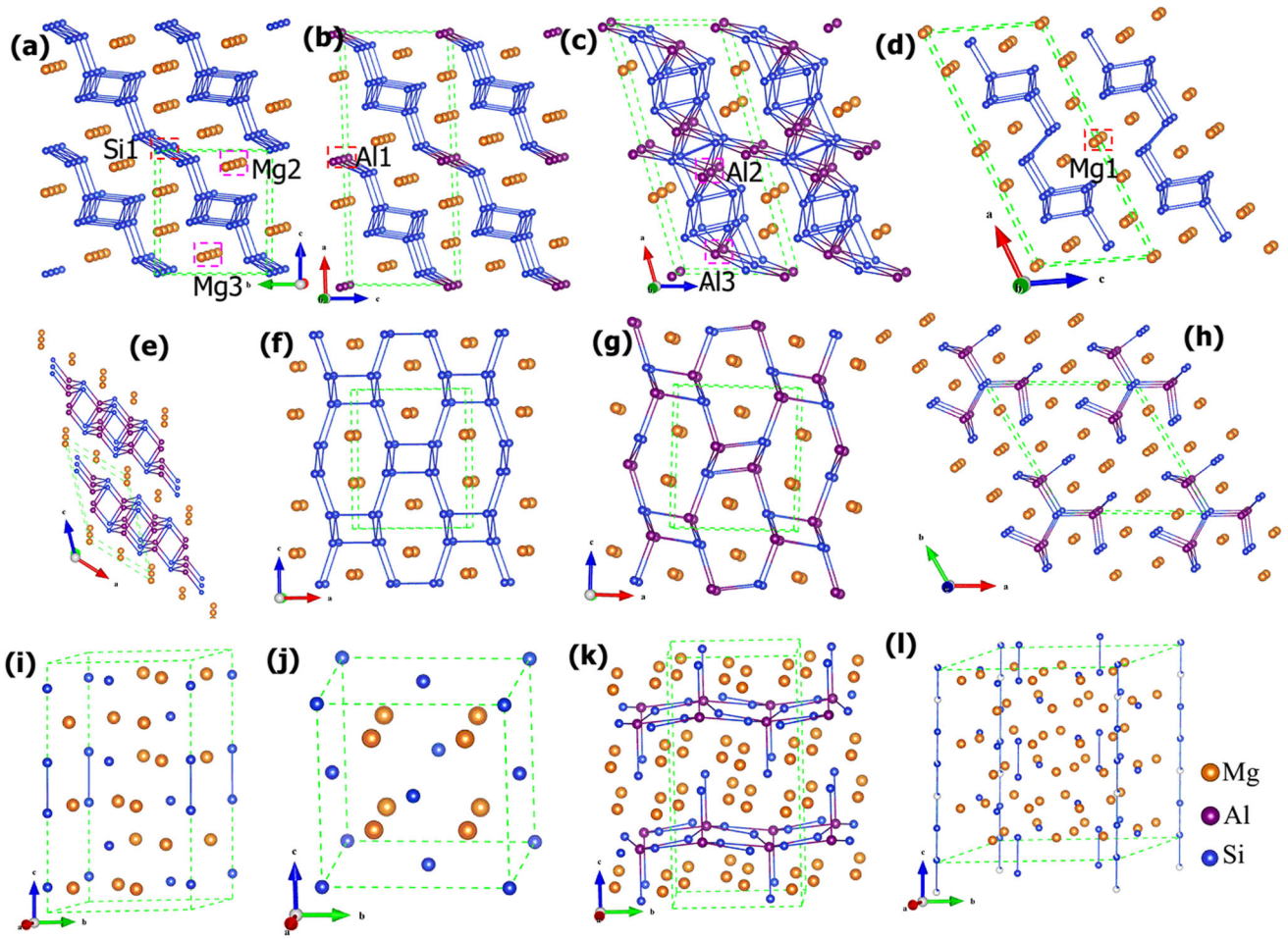

Fig. 3 (color online) Crystal structure of the precipitates in the Al–Mg–Si alloys after full stress and position relaxation. **a** $P\bar{1}$-Mg_4Si_7; **b** Mg_4AlSi_6; **c** $Mg_2Al_3Si_6$; **d** Mg_5Si_6; **e** $C2/m$-$MgAl_2Si_2$; **f** $MgSi_2$; **g** MgAlSi; **h** $Mg_9Al_3Si_7$; **i** Mg_9Si_5; **j** Mg_2Si; **k** $Pccn$-$(Mg_4AlSi_3)_{HP}$ and **l** $(Mg_9Si_5)_{HP}$

and 2.68 Å for $P\bar{1}$-type Mg_4Si_7, 2.42 and 2.55 Å for Mg_4AlSi_6, and 2.47 and 2.72 Å for $Mg_2Al_3Si_6$, correspondingly. The bond lengths of Si–Si (or Si–Al) in R-Si_4 unit (or R-Si_2Al_2 unit) in $P\bar{1}$-type Mg_4Si_7, Mg_4AlSi_6, and $Mg_2Al_3Si_6$ are 2.53, 2.70, and 2.87 Å, respectively. The close structural features imply the small barrier of the phase transformation among Mg_4Si_7, Mg_4AlSi_6, and $Mg_2Al_3Si_6$ in experiment. Additionally, the structure of Mg_5Si_6 (Fig. 3d) is also constituted with alternated layers of Si and Mg atoms, which can be derived from $P\bar{1}$-type Mg_4Si_7 with Si1 atoms substituted by Mg1 atoms.

The $C2/m$-type $MgAl_2Si_2$ (Fig. 3e) consists of bilayers of puckered graphene-like sheets of AlSi, with Mg atoms capping the puckered hexagons. The bond lengths of Si–Al within $[AlSi]_3$ six-rings are 2.49 (×2) and 2.50 (×4) Å, respectively, while the Si–Al bonds length connecting two [AlSi] layers is 2.62 Å.

In the $MgSi_2$ phase (Fig. 3f), rectangle-Si_4 units build a tightly bound bonding network, and zigzag chains of Mg atoms run through the Si channels. MgAlSi phase (Fig. 3g), close to the $MgSi_2$ structure, can be described as half of the diagonal Si atoms in the rectangle-Si_4 units substituted by Al atoms. The bond lengths of Si–Si (Si–Al) in $MgSi_2$ (in MgAlSi) are 2.45, 2.47, and 2.56 Å (2.55, 2.63 and 2.71 Å), respectively.

The crystal structure of $Mg_9Al_3Si_7$ (Fig. 3h) can be described as the linear $[Al_3Si_7]$ chains separated by Mg atoms along c direction. The Si–Al bond lengths are 2.53, 2.55, and 2.59 Å. The Si atoms in Mg_9Si_5, $(Mg_9Si_5)_{HP}$, and Mg_2Si (Fig. 3i, l, j) can be classified to three different types: isolated Si atoms, Si_2 dimers, and not fully occupied linear chains. The Si–Si bond lengths in Si_2 dimers are 2.46 Å for Mg_9Si_5, 2.46 and 2.47 Å for $(Mg_9Si_5)_{HP}$. The Si–Si bond length in linear chains in $(Mg_9Si_5)_{HP}$ is about 2.20 Å. Finally, the crystal structure of $(Mg_4AlSi_3)_{HP}$ (Fig. 3k) is composed of alternating $[AlSi_2]$ and $[Mg_4Si]$ layers, with each Al atom having five nearest Si atoms with Si–Al bond length 2.50 (×2) and 2.75 (×2) Å (within

[$AlSi_2$] layer) and 2.83 Å (between [$AlSi_2$] and [Mg_4Si] layer), and each Si atom two nearest Al atoms and one Si atom (Si–Si bond length is 2.44 Å).

Elastic properties

The calculated individual elastic constants within the strain–stress method are listed in Table 1 for different Al–Mg–Si compounds. In general, all of the mechanically stable phases show the relatively higher values of C_{11}, C_{22}, and C_{33} than that of C_{44}, indicating relatively higher incompressibility along a-, b-, and c-axis. Moreover, C_{22} (163.6 GPa) of $Mg_2Al_3Si_6$ is the largest value among the individual elastic constants, suggesting its low compressibility along b-axis. Additionally, the largest C_{44} value, 50.3 GPa, is observed in MgAlSi, indicating its relatively strong shear strength.

To further demonstrate the mechanical properties of Mg–Al–Si alloys, bulk modulus, shear modulus, Young's modulus, Poisson's ratio, and universal elastic anisotropy index (A^U) were estimated from the calculated individual elastic constants (Table 4); the previous available results are also listed for comparison. It can be seen that our calculated results are in good agreement with previously theoretical and experimental results. For example, the calculated bulk moduli of Mg_2Si and MgAlSi were 53.0 and 67.7 GPa, respectively, consistent with theoretical values reported by Anders et al., 54.3 and 69.1 GPa, respectively [15]. Also, bulk moduli of all precipitates are higher than that of pure Mg (45 GPa), but lower than that of pure Al (76 GPa) and diamond-Si (97.6 GPa). Furthermore, $MgSi_2$ exhibits highest bulk modulus, 73.1 GPa, followed by MgAlSi, 67.7 GPa, due to the strong covalent Si–Si (Si–Al) bond in three-dimensional Si-framework (Si–Al-framework). It is interesting that the bulk modulus decreased gradually with the increasing Mg concentration by the fitted function $B = 69.2 - 20.7x_{Mg}$ (as shown in Fig. 4a), possibly induced by the decreasing of the Si–Si or Si–Al covalent bonding and the increasing of the Si–Mg ionic bonding. However, there is no apparent interaction between the shear modulus and the concentration of Mg (as shown in Fig. 4b). MgAlSi possesses a maximum value, 48.8 GPa, while Mg_4AlSi_6 exhibits a minimum value, 22.0 GPa.

The ratio between the shear and bulk modulus (*B/G*) has been proposed by Pugh [42] to predict brittle or ductile behavior of materials. According to the Pugh criterion, a high *B/G* value indicates a tendency for ductility, while a low *B/G* value is associated with brittleness. From Table 4, it can be seen that *G/B* value of $Mg_2Al_3Si_6$, MgAlSi, Mg_9Si_5, and Mg_2Si are under the critical value, 1.75, separating ductility from brittleness, indicating the brittle behaviors; while the other phases are ductile, with a higher value than the critical value. The elastic anisotropy index (A^U) represents a universal measure to quantify the single-crystal elastic anisotropy. From Table 4, Mg_2Si is an isotropic phase with the lowest A^U value closed to zero (0.006), while Mg_4AlSi_6 has the largest A^U absolute value (5.09) displaying the most anisotropic.

Electronic properties

Figure 5 displays the total and partial density of states (DOS) for all the precipitates and high pressure phases. We found that Mg_2Si phase is the only phase showing the

Table 4 The bulk modulus (*B*, B_V, and B_R in GPa), shear modulus (*G*, G_V, and G_R in GPa), and Young's modulus (*E* in GPa), Poisson's ratio (υ), Pugh's ration (*B*/*G*), and universal elastic anisotropy (A^U) of Al–Mg–Si compounds compared with available experimental and theoretical results

Phase	SG	*B*	B_V	B_R	*G*	G_V	G_R	*E*	υ	*B*/*G*	A^U
pre-β″/$Mg_2Al_3Si_6$	*C*2/*m*	60.9	63.8	57.9	47.0	53.3	40.7	112.1	0.19	1.30	1.65
pre-β″/Mg_4AlSi_6	*C*2/*m*	58.8	60.3	57.2	22.0	29.3	14.6	58.6	0.33	2.67	5.09
pre-β″/Mg_4Si_7-2	$P\bar{1}$	54.9	60.4	49.4	28.2	33.5	22.8	72.2	0.28	1.95	2.57
β″/Mg_5Si_6	*C*2/*m*	61.7	63.2	60.3	34.2	39.8	28.6	86.7	0.27	1.80	2.00
U1/$MgAl_2Si_2$-12	*C*2/*m*	62.9	64.4	61.4	22.7	26.4	18.9	60.7	0.34	2.78	2.04
	$P\bar{3}m1$	71[a]									
U2/MgAlSi	*Pnma*	67.7	67.8	67.5	48.8	50.0	47.6	118.0	0.21	1.39	0.26
		69.1[a]									
U3/$MgSi_2$	*Imma*	73.1	73.3	72.9	39.2	40.4	38.1	99.8	0.27	1.86	0.31
B′/$Mg_9Al_3Si_7$	$P\bar{6}$	58.7	59.2	58.3	23.2	25.2	21.2	61.5	0.33	2.53	0.95
β′/Mg_9Si_5	$P6_3/m$	56.9	56.9	56.8	37.4	39.9	34.9	92.0	0.23	1.52	0.71
β/Mg_2Si	$Fm\bar{3}m$	53.0	53.0	53.0	43.5	43.5	43.4	102.4	0.18	1.32	0.006
		54.3[a]									
$(Mg_9Si_5)_{HP}$	$P6_3$	53.4	53.4	53.4	27.2	29.3	25.1	69.8	0.28	1.96	0.84
$(Mg_4AlSi_3)_{HP}$	*Pccn*	61.4	62.6	60.2	27.8	30.5	25.0	72.4	0.30	2.21	1.14

[a] Ref [15] from second-order Birch fit

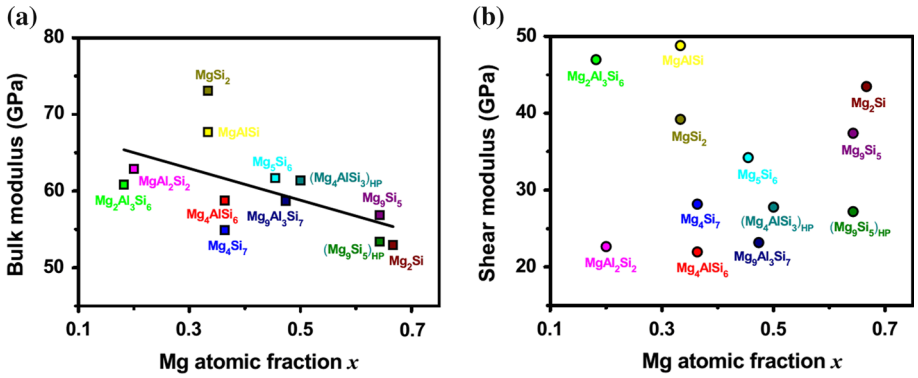

Fig. 4 (color online) Calculated bulk modulus B (in GPa) and shear modulus G (in GPa) as a function of Mg atomic fraction x

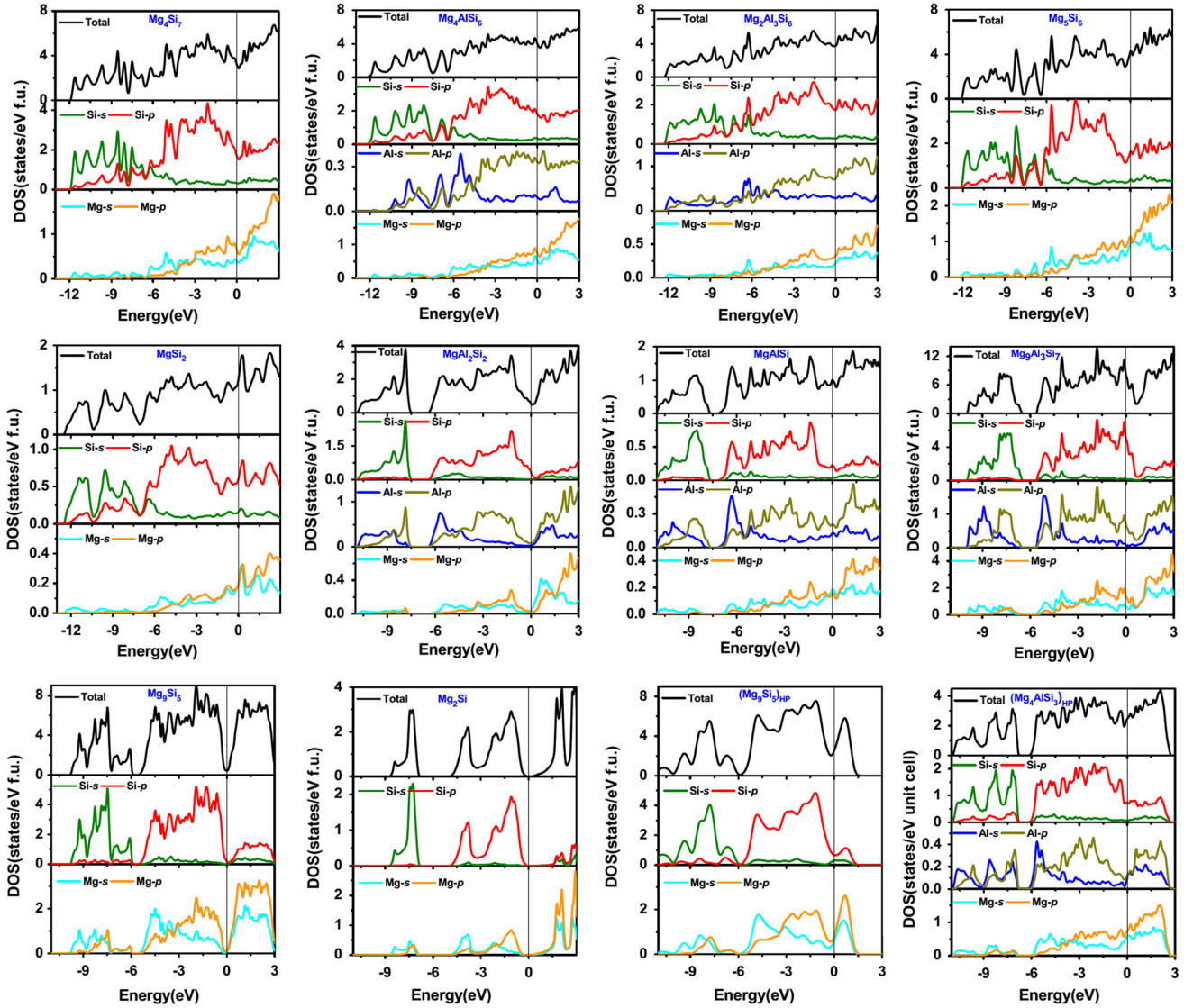

Fig. 5 (color online) Calculated total and partial density of states of the precipitates in Al–Mg–Si alloys

semiconducting feature. The calculated band structure of Mg_2Si presents an indirect gap with an energy value of 0.22 eV, in agreement with the previous theoretical results (0.23 eV) [43], but lower than experimental value, 0.74 eV [44], because of the underestimation of band gap by GGA. $P\bar{1}$-Mg_4Si_7, Mg_4AlSi_6, $Mg_2Al_3Si_6$, and Mg_5Si_6 phases

exhibit metallic features, as evidenced by finite DOS values at Fermi level (E_F), which originate mostly from 2*p* electrons of Si. The Si–Mg (or Si–Al) covenant interactions is relatively weak because of the less overlapping between the partial DOS of Si and Mg atoms (or Si and Al atoms). For $MgSi_2$, it can be found that there is a wide overlap between Si-*s* and Si-*p* from −12 to −7 eV, showing strong sp^3 hybridization, which mainly accounts for the largest bulk modulus among the considered Mg–Al–Si phases. Furthermore, there is a general feature for stable *C*2/*m*-$MgAl_2Si_2$, MgAlSi, $Mg_9Al_3Si_7$, Mg_9Si_5, Mg_2Si, *Pccn*-$(Mg_4AlSi_3)_{HP}$, and $(Mg_9Si_5)_{HP}$. Below the Fermi level, the valence bands were dominated by Si states with Si-*s* states at lower band and Si-*p* states at the higher band. Furthermore, for Mg_9Si_5 and $(Mg_9Si_5)_{HP}$, the Fermi level nearly falls in the pseudogap valley, implying more stability of these two phases than others, quite consistent with the experimental findings [8]. Nevertheless, from Fig. 5, it can be observed that, for all the Al–Mg–Si precipitated phases, the contributions to the total DOS from the Mg states are not significant because Mg atoms donate electrons to Al–Si (or Si–Si) network to stabilize the structure, for example, about 1 and 0.67–0.79 electron transformed from one Mg atom to Al–Si (or Si–Si) network for $MgAl_2Si_2$ and Mg_4Si_7, respectively, by analyzing the atomic Milliken overlap population.

The calculated DOS of lower energy structures, $P\bar{1}$-Mg_4Si_7, *C*2/*m*-$MgAl_2Si_2$, and *Pccn*-$(Mg_4AlSi_3)_{HP}$ (Fig. 6b, d, f) was compared with that of the previously proposed phases (Fig. 6a, c, e). The DOS around Fermi level (E_F) at right side is lower than that at left side in Fig. 4, and it shows a "splitting" into a pseudogap, thus underlying their stability. In $(Mg_4AlSi_3)_{HP}$ and *C*2/*m*-Mg_4Si_7, the pseudogap appears far below E_F (about 1 eV),

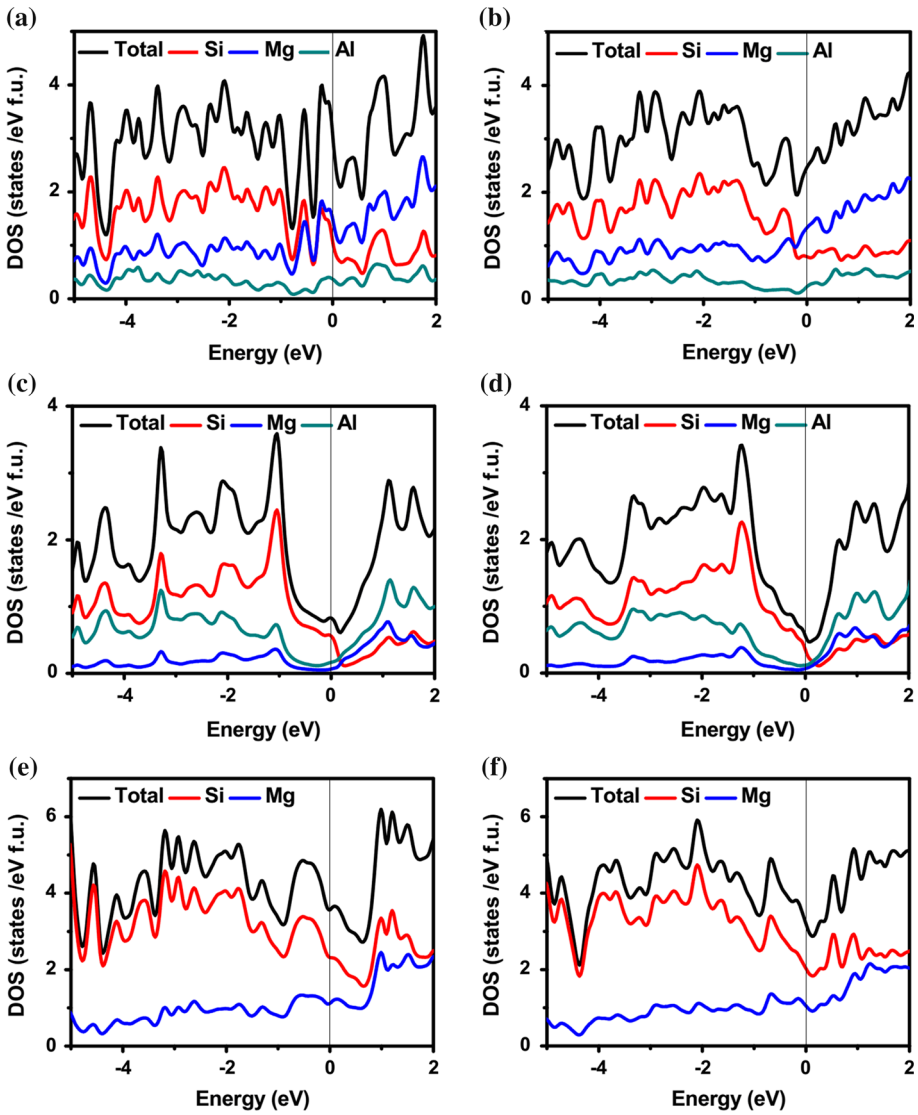

Fig. 6 (color online) Comparing total and partial density of states near Fermi level for **a** *P*4/*ncc*-$(Mg_4AlSi_3)_{HP}$; **b** *Pccn*-$(Mg_4AlSi_3)_{HP}$; **c** $P\bar{3}m1$-$MgAl_2Si_2$; **d** *C*2/*m*-$MgAl_2Si_2$; **e** *C*2/*m*-Mg_4Si_7 and **f** $P\bar{1}$-Mg_4Si_7

pointing to the electronic origin of their instability. Furthermore, for $(Mg_4AlSi_3)_{HP}$, DOS at E_F of *Pccn*-type structure Mg_4AlSi_3 was contributed more from Mg atoms than that of *P*4/*ncc*-type structure, and a similar profile between PDOS-Si and PDOS-Mg is observed, suggesting relatively stronger Si–Mg bond in *Pccn*-$(Mg_4AlSi_3)_{HP}$, thereby more favorable mechanical stability. Similarly, relatively stronger Si–Al (Si–Mg) bond for $MgAl_2Si_2$ (Mg_4Si_7) with *C*2/*m* ($P\bar{1}$) symmetry can be induced from their electronic DOS. Therefore, one can understand that the enhancement of Si–Mg (or Si–Al) bond interactions in $P\bar{1}$-Mg_4Si_7, *C*2/*m*-$MgAl_2Si_2$, and *Pccn*-$(Mg_4AlSi_3)_{HP}$ contributes to their energetic and mechanical stabilities.

Conclusions

In summary, we systematically investigated the crystal structure, phase stability, mechanical properties, and electronic structure of the precipitates and high pressure phases of in Al–Mg–Si alloys by first-principles calculations. The sequence of our calculated formation enthalpy of the precipitates is coincident with the experiment trend. Previously suggested phases *C*2/*m*-Mg_4Si_7, $P\bar{3}m$-$MgAl_2Si_2$, and *P*4/*ncc*-$(Mg_4AlSi_3)_{HP}$, are found to be mechanically unstable. The new structures of $P\bar{1}$-Mg_4Si_7, *C*2/*m*- $MgAl_2Si_2$, and *Pccn*- $(Mg_4AlSi_3)_{HP}$ are proposed in this paper. Among the precipitates, $MgSi_2$ and MgAlSi exhibit higher bulk modulus, 73.1 and 67.7GPa due to the tightly bound Si–Si/Si–Al covalent networks. MgAlSi possesses the maximum shear modulus of 48.8 GPa, and Mg_4AlSi_6 exhibits minimum shear modulus 22.0 GPa. Furthermore, the bulk modulus decreased gradually with the increase in Mg concentration by the fitted function $B = 69.2 - 20.7\ x_{Mg}$ (x, Mg atomic fraction), because of the interaction of Si–Si or Si–Al covalent bonding and ionic Si–Mg bonding.

Acknowledgements The authors acknowledge the financial support by the National Natural Science Foundation of China (NSFC) under Grants No. 51071140. The authors also thank Dr. Qingyang Hu of Carnegie institution of Washington and Dr. Jihua Hao of John Hopkins University for the improvement of the manuscript.

References

1. Edwards GA, Stiller K, Dunlop GL, Couper MJ (1998) The precipitation sequence in Al-Mg-Si alloys. Acta Mater 46:3893
2. Vissers R, van Huis MA, Jansen J, Zandbergen HW, Marioara CD, Andersen SJ (2007) The crystal structure of the β′ phase in Al–Mg–Si alloys. Acta Mater 55:3815
3. Marioara CD, Andersen SJ, Jansen J, Zandbergen HW (2003) The influence of temperature and storage time at RT on nucleation of the β″ phase in a 6082 Al-Mg-Si alloy. Acta Mater 51:789
4. Zandbergen HW, Andersen SJ, Jansen J (1997) Structure determination of Mg_5Si_6 particles in Al by dynamic electron diffraction studies. Science 277:1221
5. van Huis MA, Chen JH, Zandbergen HW, Sluiter MHF (2006) Phase stability and structural relations of nanometer-sized, matrix-embedded precipitate phases in Al–Mg–Si alloys in the late stages of evolution. Acta Mater 54:2945
6. Ravi C, Wolverton C (2004) First-principles study of crystal structure and stability of Al-Mg-Si-(Cu) precipitates. Acta Mater 52:4213
7. Matsuda K, Sakaguchi Y, Miyata Y, Uetani Y, Sato T, Kamio A, Ikeno S (2000) Precipitation sequence of various kinds of metastable phases in Al-1.0mass% Mg_2Si-0.4mass% Si alloy. J Mater Sci 35:179
8. Ji SD, Imai M, Zhu HK, Yamanaka SJ (2013) Structural characterization of magnesium-based compounds Mg_9Si_5 and Mg_4Si_3Al (superconductor) synthesized under high pressure and high temperature conditions. Inorg Chem 52:3953
9. Ringer SP, Swenser SP, Muddle BC, Polmear IJ, Sakurai T (1996) APFIM/TEM observations of a high strength-creep resistant Al-Cu-Mg-Si-Ge alloy. Mater Sci Forum 217–222:689
10. Hasting HS, Frøseth AG, Andersen SJ, Vissers R, Walmsley JC, Marioara CD, Danoix F, Lefebvre W, Holmestad R (2009) Composition of β″ precipitates in Al-Mg-Si alloys by atom probe tomography and first principles calculations. J Appl Phys 106:123527
11. Matsuda K, Gamada H, Fujii K, Uetani Y, Sato T, Kamio A, Ikeno S (1998) High-resolution electron microscopy on the Structure of Guinier-Preston Zones in an Al-1.6 Mass Pct Mg_2Si alloy. Metall Mater Trans A 29A:1161
12. Coene W, Janssen G, Beeck MOD, van Dyck D (1992) Phase retrieval through focus variation for ultra-resolution in field-emission transmission electron microscopy. Phys Rev Lett 69:3743
13. Pan RK, Ma L, Bian N, Wang MH, Li PB, Tang BY, Peng LM, Ding WJ (2013) First-principles study on the elastic properties of B′ and Q phase in Al-Mg-Si (-Cu) alloys. Phys Scr 87:015601
14. Ehlers FJH, Dumoulin S (2014) Interface configuration stability and interfacial energy for the β″ phase in Al-Mg-Si as examined with a first principles based hierarchical multi-scale scheme. J Alloys Comp 591:329
15. Frøseth AG, Høier R (2003) Bonding in MgSi and Al-Mg-Si compounds relevant to Al-Mg-Si alloys. Phys Rev B 67:224106
16. van Huis MA, Chen JH, Sluiter MHF, Zandbergen HW (2007) Phase stability and structural features of matrix-embedded hardening precipitates in Al-Mg-Si alloys in the early stages of evolution. Acta Mater 55:2183
17. Zhao D, Zhou LC, Kong Y, Wang AJ, Wang J, Peng YB, Du Y, Ouyang YF, Zhang WQ (2011) Structure and thermodynamics of the key precipitated phases in the Al-Mg-Si alloys from first-principles calculations. J Mater Sci 46:7839. doi:10.1007/s10853-011-5765-4
18. Segall MD, Lindan PJD, Probert MJ, Pickard CJ, Hasnip PJ, Clark SJ, Payne MC (2002) First-principles simulation: ideas, illustrations and the CASTEP code. J Phys Condens Matter 14:2717
19. Perdew JP, Chevary JA, Vosko SH, Jackson KA, Pederson MR, Singh DJ, Fiolhais C (1992) Atoms, molecules, solids, and surfaces: applications of the generalized gradient approximation for exchange and correlation. Phys Rev B 46:6671
20. Perdew JP, Burke K, Ernzerhof M (1996) Generalized gradient approximation made simple. Phys Rev Lett 77:3865
21. Hill R (1952) The elastic behaviour of a crystalline aggregate. Proc Phys Soc A 65:349
22. Ranganathan SI, Ostoja-Starzewski M (2008) Universal elastic anisotropy index. Phys Rev Lett 101:055504

23. Born M, Huang K (1954) Dynamical theory of crystal lattices. Oxford University Press, London
24. Wu ZJ, Zhao EJ, Xiang HP, Hao XF, Liu XJ, Meng J (2007) Crystal structures and elastic properties of superhard IrN_2 and IrN_3 from first principles. Phys Rev B 76:054115
25. Zhang H, Wang Y, Shang SL, Ravi C, Wolverton C, Chen LQ et al (2010) Solvus boundaries of (meta)stable phases in the Al-Mg-Si system: first-principles phonon calculations and thermodynamic modeling. CALPHAD 34:20
26. Kubaschewski O, Villa H (1949) Heat of formation of binary alkaline earth compounds. Z Electrochem 53:32
27. Gerstein BC, Jelinek FJ, Habenschuss M, Shickell WD, Mullaly JR, Chung PL (1967) Thermal study of groups II—IV semiconductors. Lattice heat capacities and free energies of formation. Heat capacity of Mg_2Si from 15°-300° K. J Chem Phys 47:2109
28. Blachnik R, Kunze D, Schneider A (1971) On the experimental results of a direct calorimetry method. Metall (Isernhagen) 25:119
29. Caulfield HJ, Hudson DE (1966) Sublimation in the intermetallic series $SiMg_2$, $SnMg_2$, and $PbMg_2$. Solid State Commun 4:299
30. Ryabchikov IV, Mikulinski AS (1963) Measurement of the vapor pressure of magnesium over solid magnesium and magnesium-silicon and magnesium-calcium-silicon alloys. Izv Vyssh Uchebn Zaved Tsvet Met 1:95
31. Lukashenko GM, Eremenko VN (1964) Thermodynamic properties of magnesium-silicides. Russ J Inorg Chem 9:1243
32. Rao YK, Belton GR, Gokcen NA (ed) (1981) Thermodynamic properties of Mg − Si system. Chemical metallurgy: a tribute to carl wagner. The Metallurgical Society of AIME, New York
33. Feufel H, Godecke T, Lukas HL, Sommer F (1997) Investigation of the Al-Mg-Si system by experiments and thermodynamic calculations. J Alloys Comp 247:31
34. Marioara CD, Andersen SJ, Jansen J, Zandbergen HW (2001) Atomic model for GP-zones in a 6082 Al-Mg-Si system. Acta Mater 49:321
35. Marioara CD, Nordmark H, Andersen SJ, Holmestad R (2006) Post-β'' phases and their influence on microstructure and hardness in 6xxx Al-Mg-Si alloys. J Mater Sci 41:471
36. Chen JH, Costan E, van Huis MA, Xu Q, Zandbergen HW (2006) Atomic pillar-based nanoprecipitates strengthen AlMgSi alloys. Science 312:416
37. Andersen SJ, Marioara CD, Vissers R, Frøseth A, Zandbergen HW (2007) The structural relation between precipitates in Al-Mg-Si alloys, the Al-matrix and diamond silicon, with emphasis on the trigonal phase U1-$MgAl_2Si_2$. Mater Sci Eng A 444:157
38. Andersen SJ, Marioara CD, Frøseth A, Vissers R, Zandbergen HW (2005) Crystal structure of the orthorhombic U2-$Al_4Mg_4Si_4$ precipitate in the Al-Mg-Si alloy system and its relation to the β' and β'' phases. Mater Sci Eng A 390:127
39. Wolverton C (2001) Crystal structure and stability of complex precipitate phases in Al-Cu-Mg-(Si) and Al-Zn-Mg alloys. Acta Mater 49:3129
40. Villars P, Calvert LD (1985) Pearson's handbook of crystallographic data for intermetallic phases, vol 3. American Society for Metals, Metals Park, p 2701
41. Edwards GA, Stiller K, Dunlop GL (1994) APFIM investigation of fine-scale precipitation in aluminium alloy 6061. Appl Surf Sci 76(77):219
42. Pugh SF (1954) XCII. Relations between the elastic moduli and the plastic properties of polycrystalline pure metals. Philos Mag Ser 7 45:823
43. Viennois R, Jund P, Colinet C, Tédenac JC (2012) Defect and phase stability of solid solutions of Mg_2X with an antifluorite structure: an ab initio study. J Solid State Chem 193:133
44. Mahan JE, Vantomme A, Langouche G, Becker JP (1996) Semiconducting Mg_2Si thin films prepared by molecular-beam epitaxy. Phys Rev B 54:16965